Analysis of Contra-Rotating Brushless Integrated Flux-Modulation Machine with Open-Slot Structure for Wind Power Generation

Libing Cao, *Member, IEEE,* Guanghui Yang, Yuefei Zuo, *Member, IEEE,* Yaojie He, Chenhao Zhao, Shuangchun Xie, and Christopher H. T. Lee, *Senior Member, IEEE*

***Abstract*—This paper presents a contra-rotating (CR) brushless integrated flux-modulation (BIFM) machine with open-slots structure for wind power generation, termed CR-BIFM machine. The presented machine employs two contra-rotating rotors coupled with two sets of wind turbine blades, thus being able to capture more wind energy than conventional wind turbines. Due to the dual flux-modulation effect and flux-bridge effect, the presented machine exhibits high torque/power density, making it suitable for direct-drive wind power generation without the issues related to mechanical gearboxes. As two sets of windings share the same stator slots in the presented machine, the decoupling design of windings is systematically investigated from the perspective of air-gap modulated magnetic field, considering the influence of both stator and rotors. The advantages of the presented machine are comprehensively evaluated compared to the regular machine, showing that the presented machine exhibits higher torque/power density, higher efficiency, higher power factor, and higher PM utilization. Finally, a prototype is fabricated and tested to validate the analysis.**

***Index Terms*—Contra-rotating, decoupling design, dual flux-modulation effect, flux-bridge effect, wind power generation**

I. Introduction

Wind power, as one of the cleanest renewable energy sources, is receiving ever-increasing attentions in both industry and academia. In converting wind energy into electricity, electric machine serves the enabling technology and desires high torque/power density, high efficiency, high cost-effectiveness, high reliability and low acoustic noise [1, 2]. To satisfy these performance requirements, various motor structures with distinct advantages in certain aspects have been proposed. Single-rotor machines, such as squirrel-cage induction machine [3], wound-rotor induction machine [4], doubly-fed induction machine [5], and permanent-magnet synchronous machine (PMSM) [6], are commonly adopted for wind power generation nowadays. Unfortunately, according to Betz limit, the single-rotor systems could only convert up to about 59% of the wind stream energy into useful electricity [7].

To extract wind energy more efficiently, the contra-rotating (CR) wind turbine system was developed, and experimental results indicate that this system can improve energy-extraction efficiency by about 40%, compared with the single-rotor system [8, 9]. The CR concept was initiated in the wind turbine by C. Shin in 1999 [10] and subsequently put into service in a 30 kW wind turbine [11], with the system configuration presented in Fig. 1(a). The conventional system employs the bevel-planetary gear set to transmit the combined torque and power from two CR rotor shafts to the generator. Mechanical gearboxes, however, unavoidably bear the disadvantages of the need for periodic maintenance, bulky size, loud noise, reduced reliability, and high cost. Additionally, the ratio of torque distribution on the two rotor shafts is invariable due to the fixed gear ratio of such gearboxes. Consequently, it is not feasible to implement maximum power point tracking (MPPT) control strategy on both rotor shafts [12].

To overcome the aforementioned issues, the gearless direct-drive system is developed for the CR wind turbine. The key of such system is to introduce the brushless integrated flux-modulation (BIFM) machine in the continuously variable transmission (CVT) system, which is firstly developed for hybrid electric vehicles (HEVs) [13], into wind turbines. The configuration of the gearless direct-drive system with the CR wind turbine is shown in Fig. 1(b). The CR-BIFM machine is the enabling technology to realize the CVT function and gearless direct-drive operation. Its inner and outer rotors are coupled with the auxiliary and main blades that rotate with the flow of wind in counter-clockwise and clockwise directions, respectively. Different from the operation condition of the BIFM machine in HEVs, two rotors of the BIFM machine in wind turbines should always rotate in contrary directions to induce higher voltage and hence harvesting more wind energy. Besides, two sets of windings also provide the flexibility of torque control between two rotors. Thus, the dual MPPT control can be realized to enable maximum efficiency of wind power conversion [12].

In recent years, various BIFM machines with the integration of the PMSM part and magnetic-geared machine (MGM) part in a single machine have been developed. In [14, 15], a BIFM machine with the spoke-PM outer rotor and the surface-PM inner rotor is developed. Compared with the conventional BIFM machine with only the surface-PM inner rotor, the developed BIFM machine presents higher torque/power density due to improved torque from the PMSM part. However, its PM utilization is sacrificed due to lower torque of the MGM part under higher PMs consumption. To resolve this issue, the salient-pole inner rotor is introduced in the BIFM machine [16]. This structure saves PMs consumption and improves the torque of the MGM part by reducing equivalent airgap length. However, the split-tooth stator in the aforementioned machines reduces the equivalent airgap radius and aggravates the flux leakage in the auxiliary teeth. Thus, the torque density and power factor are still relatively low. Furthermore, the regular stator teeth are adopted in the BIFM machines [12, 17, 18], where the PMs are both inserted in the inner rotor and outer rotor and form the so-called bidirectional flux-modulation

effect to enhance torque/power density. Compared with the conventional BIFM machine, these machines exhibit higher torque/power density but lower PM utilization. Very recently, a BIFM machine with open-slot auxiliary teeth is developed in such a way that the PM vernier machine (PMVM) part is introduced to replace the PMSM part in the BIFM machine [19]. As a result, torque/power density is improved due to the enhanced flux-modulation effect of the PMVM part. However, the power factor of the machine is low due to the split-tooth stator. Besides, the influence of stator and rotors on the mutual coupling of two sets of windings is not considered, while the flux-bridge effect is not investigated and revealed.

In this paper, a CR-BIFM machine with open-slot structure, is developed for wind power generation. The presented machine features the dual flux-modulation effect and flux-bridge effect, thus exhibiting higher torque/power density, higher efficiency, higher power factor, and higher PM utilization than the regular CR-BIFM machine. The coupling analysis of two sets of windings, considering the influence of both stator and rotors, is systematically investigated from the perspective of airgap modulated magnetic field to provide guidance in low-coupling designs. Finally, a prototype is manufactured and tested to validate the analysis.

II. Machine Topology and Working Principle

A. Machine Topology

Fig. 2 (a) and (b) show the topologies of the regular CR-BIFM machine [12, 18] and the presented CR-BIFM one. In the regular machine, the dual-PM structure with PMs placed both in inner and outer rotors is developed to provide the so-called bidirectional flux modulation effect for torque/power improvement. Specifically, both the iron poles of the inner rotor and steel segments in the outer rotor act as the flux modulators, modulating the PMs of the outer and inner rotors, respectively. Two sets of windings are placed in the stator with regular semi-closed slots. Hence, the regular machine can be decomposed into two parts, namely the PMSM part consisting of winding I, the outer rotor and stator, and the MGM part consisting of winding II, the inner rotor, outer rotor, and stator.

By contrast, the presented machine is composed of the PMVM part and MGM part, where the former one is composed of winding I, outer rotor with spoke-array PMs, and stator with open slots, and the latter one is composed of winding II, the inner rotor, outer rotor and stator with open slots. Since both PMVM and MGM parts provide inherent magnetic gearing effects, the presented machine exhibits dual flux-modulation effect to boost torque/power density. Meanwhile, the salient-pole inner rotor can function as the magnetic bridge to increase the flux density of pole-pair number of winding I. Thus, the flux bridge effect existing in the PMVM part can further enhance the torque/power density of the presented machine.

B. Working Principle

1) PMVM Part

Based on the flux-modulation theory, the number of the stator slots Q_s, the pole-pair number of PMs in the outer rotor P_{or}, and the pole-pair number of winding I P_{WI} should follow

$$Q_s = P_{or} + P_{WI} \tag{1}$$

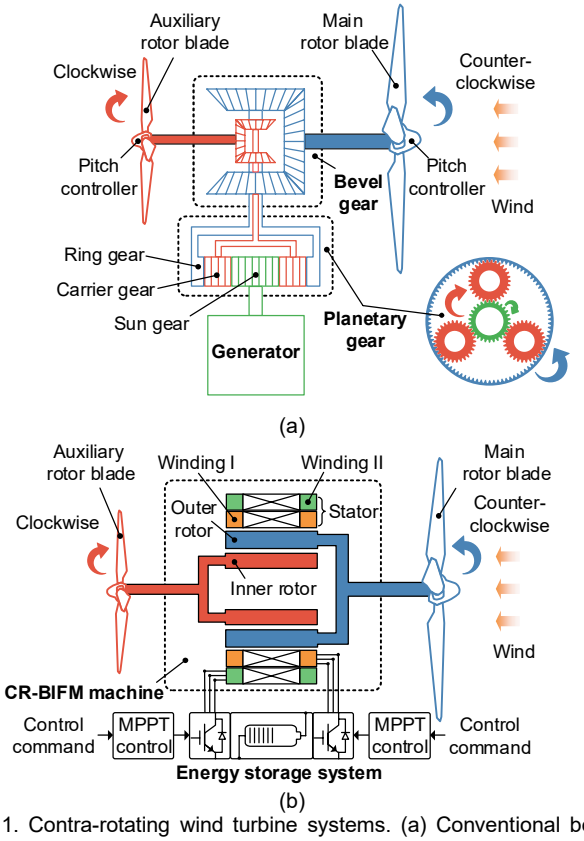

Fig. 1. Contra-rotating wind turbine systems. (a) Conventional bevel-planetary gear-based system. (b) Proposed gearless direct-drive system.

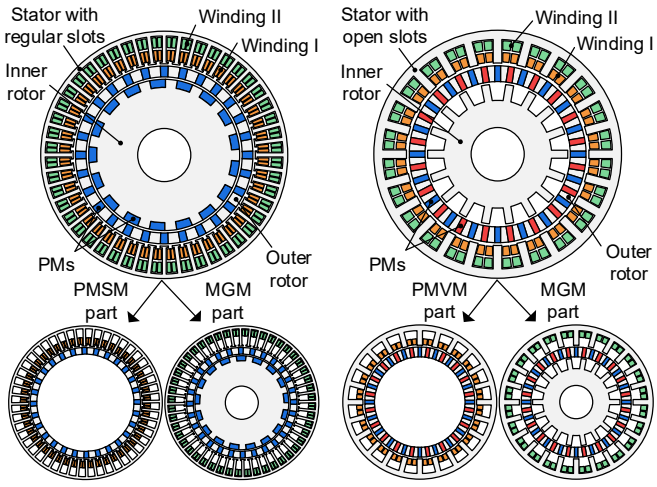

Fig. 2. Topologies of CR-BIFM machines. (a) Regular design [12, 18]. (b) Presented design.

Besides, the torque of outer rotor due to winding I T_{or_WI} and the torque of winding I on the stator T_{WI} have the relation as

$$T_{or\_WI} = -P_{or}/P_{WI}\, T_{WI} = G_{or\_WI} T_{WI} \tag{2}$$

where $G_{or\_WI} = -P_{or}/P_{WI}$ is the gear ratio between outer rotor and winding I. Compared to T_{WI}, the magnetic-gearing (or vernier effect) of PMVM part can boost T_{or_WI} with a given gear ratio.

2) MGM Part

Based on the flux-modulation theory, the pole-pair of PMs in the outer rotor P_{or}, the number of salient poles in the inner rotor P_{ir}, and the pole-pair number of winding II P_{WII} should satisfy

$$P_{or} = P_{ir} + P_{WII} \tag{3}$$

Besides, the torques developed in inner rotor T_{ir_WII} and outer rotor T_{or_WII} due to winding II, as well as the torque of winding II on the stator T_{WII} comply with the relation as

$$T_{or\_WII} = -P_{or}/P_{WII}\, T_{WII} = G_{or\_WII} T_{WII} \tag{4}$$

$$T_{ir\_WII} = P_{ir}/P_{WII}\, T_{WII} = G_{ir\_WII} T_{WII} \tag{5}$$

where $G_{or\_WII} = -P_{or}/P_{WII}$ is the gear ratio between outer rotor and winding II, and $G_{ir\_WII} = P_{ir}/P_{WII}$ is the gear ratio between inner rotor and winding II. Compared to T_{WII}, magnetic gearing of MGM part can boost both the T_{or_WII} and T_{ir_WII} with the corresponding gear ratios.

3) *Integration of Two Machine Parts*

The total torque of stator T_{st}, outer rotor T_{or}, and inner rotor T_{ir} in the presented machine can be expressed as

$$T_{st} = T_{WI} + T_{WII} \tag{6}$$

$$T_{or} = T_{or\_WI} + T_{or\_WII} = G_{or\_WI} T_{WI} + G_{or\_WII} T_{WII} \tag{7}$$

$$T_{ir} = T_{ir\_WII} = G_{ir\_WII} T_{WII} \tag{8}$$

Eqs. (6) to (8) show that all the torque components T_{WI} and T_{WII} in stator are amplified by the gear ratios to develop higher torque components in the rotors due to the dual flux-modulation effect. It can improve the torque/power density, which is highly preferable for the direct-drive wind turbine.

III. Analysis of Decoupling Effect on Windings

Since two sets of windings share the same stator slots in BIFM machines, more attentions should be paid on the decoupling design of windings. Otherwise, additional induced voltage and circulating current might complicate the system control, incur larger torque ripple, and even cause deterioration of the whole system. In [14], the decoupling effect on windings is analyzed from the perspective of periodicity and anti-periodicity of windings. This method is suitable for the BIFM machines having inner rotors with surfaced-mounted PMs but not effective for those with salient poles. In [19], the decoupling effect of two windings is analyzed with consideration of the direct coupling of windings, but the stator and rotors, which have significant influence on the coupling of windings, are not taken into account. In this section, the decoupling of windings is analyzed from the perspective of air-gap modulated magnetic field and the influence of both stator and rotors on decoupling is considered. The method developed in this paper is generic and can be applied to other types of BIFM machines as well as those machines with multiple sets of windings.

Without loss of generality, the induced flux linkage and voltage of winding II due to the sole excitation of winding I are calculated to analyze the decoupling of two winding sets. Based on winding function theory, the flux linkage that links winding II $\Psi_{w,II}$ due to sole excitation of winding I can be expressed as

$$\Psi_{w,II} = L_s R_g \int_0^{2\pi} B_{w,I}(\theta) N_{w,II}(\theta)\, d\theta \tag{9}$$

where L_s is stack length, R_g is the outer air-gap radius, θ is mechanical angular position; $B_{w,I}(\theta)$ is the magnetic flux density in the outer airgap solely produced by winding I without PMs excitation; $N_{w,II}(\theta)$ is the winding function of winding II.

The permeance of stator with open slots can be expressed as

$$\Lambda_s(\theta) = \sum_{i=0,1,2}^{\infty} \Lambda_{s,i} \cos\left(iQ_s\left(\theta - \theta_{s,0}\right)\right) \tag{10}$$

where $\Lambda_{s,i}$ is the i-th order permeance of stator and $\theta_{s,0}$ is its initial mechanical angular position. The permeance of the outer rotor with modulators can be expressed as

$$\Lambda_{or}(\theta) = \sum_{j=0,1,2}^{\infty} \Lambda_{or,j} \cos\left(j2P_{or}\left(\theta - \theta_{or,0}\right)\right) \tag{11}$$

where $\Lambda_{or,j}$ is the jth-order permeance of the outer rotor and $\theta_{or,0}$ is its initial mechanical angular position. The permeance of the inner rotor with salient poles can be expressed as

$$\Lambda_{ir}(\theta) = \sum_{k=0,1,2}^{\infty} \Lambda_{ir,k} \cos\left(kP_{ir}\left(\theta - \theta_{ir,0}\right)\right) \tag{12}$$

where $\Lambda_{ir,k}$ is the kth-order permeance of the inner rotor and $\theta_{ir,0}$ is its initial mechanical angular position.

Then, magnetic flux density $B_{w,I}(\theta)$ in (9) is calculated as

$$\begin{aligned} B_{w,I}(\theta) &= \frac{3\sqrt{2}N_{ph,I}I_{rms,I}}{\pi} \sum_{h=1,2,3}^{\infty} \frac{k_{h,I}}{t_{c,I}} \cos\left(ht_{c,I}\theta \pm \omega_e t\right) \\ &\quad \times \Lambda_s(\theta)\Lambda_{or}(\theta)\Lambda_{ir}(\theta) \\ &= \sum_{h=1,2,3}^{\infty}\sum_{i=0,1,2}^{\infty}\sum_{j=0,1,2}^{\infty}\sum_{k=0,1,2}^{\infty} \frac{3\sqrt{2}N_{ph,I}I_{rms,I}}{8\pi} \frac{k_{h,I}}{t_{c,I}} \Lambda_{s,i}\Lambda_{or,j}\Lambda_{ir,k} \\ &\quad \times \cos\begin{pmatrix} \left(ht_{c,I} \pm iQ_s \pm j2P_{or} \pm kP_{ir}\right)\theta \pm \omega_e t \\ \mp iQ_s\theta_{s,0} \mp j2P_{or}\theta_{or,0} \mp kP_{ir}\theta_{ir,0} \end{pmatrix} \end{aligned} \tag{13}$$

where $N_{ph,I}$ is the number of turns per phase in series of winding I; $I_{rms,I}$ is the RMS value of current of winding I; $k_{h,I}$ is the winding factor of hth-order MMF harmonic by winding I; ω_e is the electrical angular speed of winding I; $t_{c,I} = \mathrm{GCD}(Q_s, P_{w,I})$ is the machine periodicity of winding I (note: GCD is the greatest common divisor).

Besides, the winding function of winding II $N_{w,II}(\theta)$ can be expressed as

$$N_{w,II}(\theta) = \frac{2N_{ph,II}}{\pi} \sum_{n=1,2,3} \frac{k_{n,II}}{nt_{c,II}} \cos\left(nt_{c,II}\theta\right) \tag{14}$$

where $N_{ph,II}$ is the number of turns per phase in series of winding II; $k_{n,II}$ is the winding factor of nth-order MMF harmonic by winding II; $t_{c,II} = \mathrm{GCD}(Q_s, P_{w,II})$ is the machine periodicity of winding II.

By substituting (13) and (14) into (9), the flux linkage $\Psi_{w,II}$ can be obtained. According to the orthogonality property of trigonometric functions, the pole-pair numbers of harmonics in $B_{w,I}(\theta)$ and $N_{w,II}(\theta)$ in (9) should be unequal in such a way that the mutual flux linkage $\Psi_{w,II}$ between winding I and winding II is theoretically zero, i.e., these two sets of windings are decoupled. More specifically, let $H_{w,I}$ and $H_{w,II}$ denote the sets containing all the pole-pair numbers of harmonics in $B_{w,I}(\theta)$ in (13) and $N_{w,II}(\theta)$ in (14) respectively, the intersection of $H_{w,I}$ and $H_{w,II}$ should be empty, i.e., $H_{w,I} \cap H_{w,II} = \varnothing$ to realize the decoupling of two sets of windings.

To facilitate the analysis, the decoupling of two windings is first investigated without consideration of the inner rotor. Afterwards, the effect of inner rotor on the decoupling of two winding is studied.

A. Without Consideration of the Inner Rotor

When the modulation of the inner rotor is not considered, Λ_{ir} in (12) should only have constant permeance, and thus k in (12) and (13) should be zero. Then, according to (13) and (14), the sets $H_{w,I}$ and $H_{w,II}$ can be summarized in a general form as listed

in Table I. As $ht_{c,I}$ and $nt_{c,II}$ are dependent on the parity of $Q_s/t_{c,I}$ and $Q_s/t_{c,II}$, respectively. Hence, the decoupling analysis of two sets of windings can be decomposed into four types: 1) both $Q_s/t_{c,I}$ and $Q_s/t_{c,II}$ are even (i.e., Type-I); 2) $Q_s/t_{c,I}$ is even and $Q_s/t_{c,II}$ is odd (i.e., Type-II); 3) $Q_s/t_{c,I}$ is odd and $Q_s/t_{c,II}$ is even (i.e., Type-III); 4) both $Q_s/t_{c,I}$ and $Q_s/t_{c,II}$ are odd (i.e., Type-IV).

1) *Both $Q_s/t_{c,I}$ and $Q_s/t_{c,II}$ are Even (Type-I)*

When both $Q_s/t_{c,I}$ and $Q_s/t_{c,II}$ are even, two sets of windings are decoupled if integers a and b are not both odd, where a and b are mutually prime, $a=t_{c,I}/g$, $b=t_{c,II}/g$, and g=GCD ($t_{c,I}$, $t_{c,II}$).

Proof: When both $Q_s/t_{c,I}$ and $Q_s/t_{c,II}$ are even, the harmonic pole-pairs $ht_{c,I}$ for winding I and $nt_{c,II}$ for winding II only contains odd times of corresponding machine periodicity [20]. In such case, it yields

$$ht_{c,I} = (2k-1)t_{c,I}, \quad k = 1,2,3... \tag{15}$$

$$nt_{c,II} = (2l-1)t_{c,II}, \quad l = 1,2,3... \tag{16}$$

Then, harmonic sets $H_{w,I}$ and $H_{w,II}$ in Table I can be rewritten as

$$\begin{cases} H_{w,I} = \left|(2k-1)t_{c,I} \pm iQ_s \pm j2P_{or}\right| \\ H_{w,II} = (2l-1)t_{c,II} \end{cases} \tag{17}$$

According to the definition of $t_{c,I}$ and (1), P_{or} is always the multiple of $t_{c,I}$ and thus the multiple of g = GCD ($t_{c,I}$, $t_{c,II}$). As $Q_s/t_{c,I}$ is even, Q_s is even multiple of $t_{c,I}$ and thus even multiple of g. Then, $H_{w,I}$ and $H_{w,II}$ in (17) can be further rewritten as

$$\begin{cases} H_{w,I} = \left|(2k-1)a \pm 2i' \pm 2j'\right|g, \quad i', j' = 0,1,2,3... \\ H_{w,II} = (2l-1)bg \end{cases} \tag{18}$$

It can be seen that $H_{w,I}$ and $H_{w,II}$ in (18) have no intersection ($H_{w,I} \cap H_{w,II} = \varnothing$) only when a and b are not both odd. Thus, when both $Q_s/t_{c,I}$ and $Q_s/t_{c,II}$ are even, two sets of windings are decoupled if integers a and b are not both odd.

2) *$Q_s/t_{c,I}$ is Even and $Q_s/t_{c,II}$ is Odd (Type-II)*

When $Q_s/t_{c,I}$ is even and $Q_s/t_{c,II}$ is odd, two sets of windings are decoupled if integers a is odd and b is even, where a and b are mutually prime, $a=t_{c,I}/g$, $b=t_{c,II}/g$, and g=GCD ($t_{c,I}$, $t_{c,II}$).

Proof: When $Q_s/t_{c,I}$ is even and $Q_s/t_{c,II}$ is odd, relation (15) still holds. Then, $H_{w,I}$ and $H_{w,II}$ can be rewritten as

$$\begin{cases} H_{w,I} = \left|(2k-1)t_{c,I} \pm iQ_s \pm j2P_{or}\right| \\ H_{w,II} = nt_{c,II} \end{cases} \tag{19}$$

According to the definition of $t_{c,I}$ and (1), P_{or} is the multiple of g = GCD ($t_{c,I}$, $t_{c,II}$), while Q_s is even multiple of g since $Q_s/t_{c,I}$ is even. Then, $H_{w,I}$ and $H_{w,II}$ in (19) can be further rewritten as

$$\begin{cases} H_{w,I} = \left|(2k-1)a \pm 2i' \pm 2j'\right|g, \quad i', j' = 0,1,2,3... \\ H_{w,II} = nbg \end{cases} \tag{20}$$

It can be seen that $H_{w,I}$ and $H_{w,II}$ in (20) have no intersection ($H_{w,I} \cap H_{w,II} = \varnothing$) only when a is odd and b is even. Thus, when both $Q_s/t_{c,I}$ is even and $Q_s/t_{c,II}$ is odd, two sets of windings are decoupled if integers a is odd and b is even,

3) *$Q_s/t_{c,I}$ is Odd and $Q_s/t_{c,II}$ is Even (Type-III)*

When $Q_s/t_{c,I}$ is odd and $Q_s/t_{c,II}$ is even, two sets of windings are decoupled if integers a is even and b is odd, where a and b are mutually prime, $a=t_{c,I}/g$, $b=t_{c,II}/g$, and g=GCD ($t_{c,I}$, $t_{c,II}$).

Proof: When $Q_s/t_{c,I}$ is even and $Q_s/t_{c,II}$ is odd, relation (16) still holds. Then, $H_{w,I}$ and $H_{w,II}$ can be rewritten as

TABLE I
POLE-PAIR NUMBERS OF HARMONICS OF WINDINGS

Condition	$H_{w,I}$	$H_{w,II}$
Without consideration of the inner rotor	$\lvert ht_{c,I} \pm iQ_s \pm j2P_{or}\rvert$ h =1, 2, 3, 4… i, j=0, 1, 2, 3…	$nt_{c,II}$ n =1, 2, 3, 4…
With consideration of the inner rotor	$\lvert ht_{c,I} \pm iQ_s \pm j2P_{or} \pm kP_{ir}\rvert$ h =1, 2, 3, 4… i, j, k =0, 1, 2, 3…	$nt_{c,II}$ n =1, 2, 3, 4…

$$\begin{cases} H_{w,I} = \left|ht_{c,I} \pm iQ_s \pm j2P_{or}\right| \\ H_{w,II} = (2l-1)t_{c,II} \end{cases} \tag{21}$$

According to the definition of $t_{c,I}$ and (1), P_{or} is the multiple of g = GCD ($t_{c,I}$, $t_{c,II}$), while Q_s is even multiple of g since $Q_s/t_{c,II}$ is even. Then, $H_{w,I}$ and $H_{w,II}$ in (21) can be further rewritten as

$$\begin{cases} H_{w,I} = \left|ha \pm 2i' \pm 2j'\right|g, \quad i', j' = 0,1,2,3... \\ H_{w,II} = (2l-1)bg \end{cases} \tag{22}$$

It can be seen that $H_{w,I}$ and $H_{w,II}$ in (22) have no intersection ($H_{w,I} \cap H_{w,II} = \varnothing$) only when a is even and b is odd. Thus, when both $Q_s/t_{c,I}$ is odd and $Q_s/t_{c,II}$ is even, two sets of windings are decoupled if integers a is even and b is odd.

4) *Both $Q_s/t_{c,I}$ and $Q_s/t_{c,II}$ are Odd (Type-IV)*

When both $Q_s/t_{c,I}$ and $Q_s/t_{c,II}$ are odd, $H_{w,I}$ and $H_{w,II}$ in Table I will always have intersection, i.e., $H_{w,I} \cap H_{w,II} \neq \varnothing$, showing that there exists no possibility to decouple two sets of windings.

B. With Consideration of the Inner Rotor

When the inner rotor is considered, the harmonic set $H_{w,I}$ in Table I has the additional kP_{ir} component due to the modulation of inner rotor. The decoupling analysis of two sets of windings can be analyzed in the same way as Part A, while the detailed derivation is omitted for the sake of brevity. It is proved that a and b should not be both odd while P_{ir} should be a multiple of $2g$ to decouple two windings. However, these two conditions contradict each other and cannot be simultaneously satisfied, while the contradiction is proven as follows.

Proof: When a and b are not both odd, $t_{c,I}$ and $t_{c,II}$ are not both odd and thus Q_s is even multiple of g. When P_{ir} is a multiple of $2g$, we have the following relationships

$$P_{or} = ug;\ P_{ir} = 2vg;\ Q_s = 2wg, \quad u, v, w \in \mathbb{Z}^+ \tag{23}$$

$$P_{WI} = Q_s - P_{or} = (2w-u)g;\ P_{WII} = P_{or} - P_{ir} = (u-2v)g \tag{24}$$

According to the definition of $t_{c,I}$ and $t_{c,II}$, we have

$$\begin{aligned} t_{c,I} &= \mathrm{GCD}(Q_s, P_{WI}) = \mathrm{GCD}\left(2wg, (2w-u)g\right) \\ &= \mathrm{GCD}(2w, u) \times g = ag \end{aligned} \tag{25}$$

$$\begin{aligned} t_{c,II} &= \mathrm{GCD}(Q_s, P_{WII}) = \mathrm{GCD}(2wg, (u-2v)g) \\ &= \mathrm{GCD}(2w, u-2v) \times g = bg \end{aligned} \tag{26}$$

Eqs. (25) and (26) lead to

$$a = \mathrm{GCD}(2w, u);\ b = \mathrm{GCD}(2w, u-2v) \tag{27}$$

Since a and b are mutually prime numbers, u must be an odd number while a and b should be both odd numbers according to (27). However, this contradicts the prerequisite that a and b are not both odd. Therefore, the condition that a and b are both odd and the condition that P_{ir} is a multiple of $2g$ cannot be satisfied simultaneously.

The aforementioned analysis shows that when the inner rotor is considered, two windings are always coupled theoretically

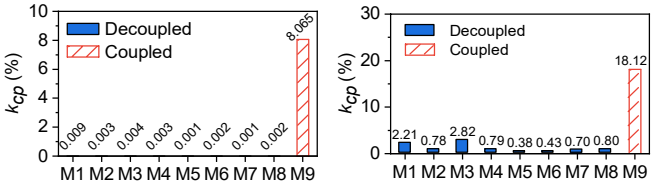

Fig. 3. Degrees of coupling. (a) Without inner rotor. (b) With inner rotor

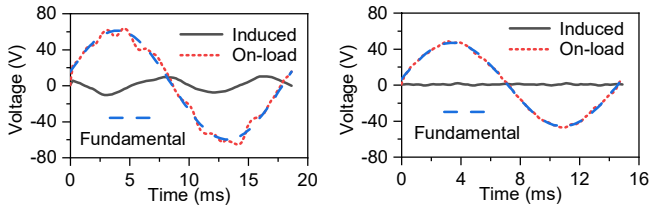

Fig. 4. Voltage waveforms. (a) Coupled design M9. (b) Decoupled design M3.

due to the modulation of inner rotor. However, with careful selection of slot-pole combination, the coupling degree of two windings can be negligible. Firstly, the slot-pole combinations should obey the decoupling conditions in Part A when the inner rotor is not considered. Secondly, when the effect of inner rotor is considered, the dominant harmonics in the in the outer airgap are taken into account to analyze the degree of coupling. As winding I has the pole-pair number of P_{WI}, the dominant harmonics due to the modulation of stator should be P_{WI} and slot harmonic Q_s-P_{WI}. In the presented machine, Q_s-P_{WI} is larger than P_{ir}, according to (1) and (3). Therefore, the Q_s-P_{WI} harmonic will mainly go through the outer airgap and the outer rotor, rather than the inner airgap and inner rotor, because the magnetic reluctance of Q_s-P_{WI} harmonic is lower through the former. As a result, only slot harmonic P_{WI} becomes the dominant harmonic influenced by the modulation of inner rotor. Considering the modulation of stator slots, outer rotor and inner rotor, the dominant harmonic set $dH_{w,I}$ of winding I can be expressed as

$$dH_{w,I} = \left|P_{WI} \pm j2P_{or} \pm P_{ir}\right|, i, j = 0,1 \tag{28}$$

Let $dH_{w,I,II}$ become the harmonic sets containing the same harmonics in $dH_{w,I}$ and $H_{w,II}$, i.e., $dH_{w,I,II}$=$dH_{w,I} \cap H_{w,II}$, the lowest order of harmonics in $dH_{w,I,II}$ can be calculated with reference to the pole-pair P_{WII} of winding II and denoted as n_L. Thus, high value of n_L (i.e., above 3) means that harmonic sets $dH_{w,I}$ and $H_{w,II}$ will only intersect in high-order harmonics coupled by winding II. Considering low amplitudes of high-order harmonics, the coupling degree of two sets of windings is expected to be low when n_L is larger than 3. Hence, two sets of windings can be considered as decoupled.

When the number of stator slots Q_s is relatively large, it is desired that P_{or} and P_{ir} are large enough to be close to Q_s. Thus, a large gear ratio can be maintained in the PMV and MGM parts in the presented machine. As a result, according to (28), the order of harmonics in $dH_{w,I}$ will be much larger than P_{WII}, i.e., the value of n_L will be larger than 3. In such a case, the coupling degree of two sets of windings is low and two sets of windings can be considered as decoupled in the presented machine.

C. Validation of Decoupling Analysis

To indicate the coupling degree of two sets of windings, the variable k_{cp} is defined as

$$k_{cp} = \max(V_{ind,I}/V_{on,I}, V_{ind,II}/V_{on,II}) \tag{29}$$

where $V_{ind,I}$ (and $V_{ind,II}$) is the maximal amplitude of induced voltage of winding I (and II) due to winding II (and I) excitation only, $V_{on,I}$ (and $V_{on,II}$) is the fundamental amplitude of on-load voltage of winding I (and II) due to both winding I (and II) excitation and PMs.

The coupling degree k_{cp} without considering the inner rotor is firstly analyzed. Without loss of representativeness, eight machines (i.e., M1-M8) covering all the decoupled types from Type-I to Type-III are investigated, while the details of M1-M8 are summarized in Table II. Specifically, Type-I decoupling includes M3; Type-II decoupling includes M2, M5 and M8; and Type-III decoupling includes M1, M4, M6, and M7. As a comparison, a coupled design with Q_s=18, P_{or}=16, P_{in}=12 (denoted as M9, 18s16p12p) that belongs to Type-IV is also analyzed. Note that this part aims to validate the decoupling analysis while the selection of optimal slot-pole combinations will be studied in Section IV. Fig. 3(a) shows the coupling degree of M1-M9 with the outer rotor rotating in clockwise at rated 200 r/min. As can be seen, the coupling degree of decoupled designs M1-M8 is almost zero, i.e., it is much smaller than that of coupled design M9. The result agrees well with the analysis in Part A.

When the inner rotor is considered, the coupling degree of M1-M9 designs is also analyzed. At rated conditions, the outer rotor rotates in clockwise with 200 r/min and inner rotor rotates in counter-clockwise with 300 r/min, while the coupling degree is summarized in Fig. 3(b). Due to the modulation effect of inner rotor, the coupling degrees of all machines are increased. However, M1-M8 machines still exhibit almost negligible coupling degree, i.e., the values are much smaller than that of M9 design. In this case, M1-M8 designs can be considered as

TABLE II
SLOT-POLE COMBINATIONS OF THE PRESENTED MACHINES

Machine	Q_s	$P_{w,I}$	$P_{w,II}$	P_{or}	P_{ir}	k_{WI}	k_{WII}	G_{rI}	G_{rII}	n_L
M1	18	2	3	16	13	0.95	1	8	5.3	5
M2	18	3	2	15	13	1	0.95	5	7.5	5
M3	**24**	**4**	**2**	**20**	**18**	**1**	**0.97**	**5**	**10**	**7**
M4	30	4	5	26	21	0.91	1	6.5	5.2	5
M5	30	5	4	25	21	1	0.91	5	6.3	4
M6	36	4	5	32	27	0.95	0.92	8	6.4	19
\	36	4	6	32	26	0.95	1	8	5.3	5
M7	36	5	4	31	27	0.92	0.95	6.2	7.75	8
\	36	5	6	31	25	0.92	1	6.2	5.2	5
M8	36	6	3	30	27	1	0.97	5	10	7
\	36	6	4	30	26	1	0.95	5	7.5	5
\	36	6	5	30	25	1	0.92	5	6	∞

TABLE III
MAIN PERFORMANCES OF THE PRESENTED MACHINES

Machine	M1	M2	**M3**	M4	M5	M6	M7	M8
T_{rip_outer} (%)	9.0	18.1	**13.9**	15.0	14.7	20.4	8.0	17.2
T_{rip_inner} (%)	67.3	35.9	**28.9**	147.7	103.0	137.7	141.9	95.2
T_{av_outer} (Nm)	69.5	70.8	**83.8**	59.3	60.0	62.1	65.4	73.6
T_{av_inner} (Nm)	21.4	31.7	**45.1**	17.7	22.2	18.7	20.8	36.2
P_{f_WI}	0.97	0.99	**0.99**	0.99	0.99	0.97	0.99	0.99
P_{f_WII}	0.93	0.89	**0.86**	0.89	0.91	0.86	0.86	0.86
UMF	✓	✓	×	✓	✓	✓	✓	✓

Note: T_{rip_outer} and T_{rip_inner} are peak-to-peak torque ripple; T_{av_outer} and T_{av_inner} are average steady torque of outer rotor and inner rotor, respectively; P_{f_WI} and P_{f_WII} are power factor of winding I and winding II, respectively;

decoupled. This phenomenon is mainly due to high value of n_L (i.e., above 3) as shown in Table II, i.e., the effect of inner rotor of M1-M8 designs is negligible. Taking decoupled design M3 and coupled design M9 as exemplification, the induced voltages of winding I due to only winding II excitation, the on-load voltages of winding I due to winding II excitation and PMs, and its fundamental components are presented in Fig. 4. The ratio of the induced voltage to the fundamental on-load voltage in M9 design is much larger than that in M3 design, leading to sharp different of coupling degree k_{cp} between two designs. Based on the aforementioned analysis, the decoupling design of windings is validated.

IV. Selection of Slot-Pole Combination

As different slot-pole combinations contribute different winding factors and gear ratios that have paramount influence on the machine performances, it is of necessity to filter out undesirable slot-pole combinations. Generally, higher gear ratios produce higher output torque but also sacrifice power factor. Thus, the gear ratios are restrained from 5 to 10 to avoid poor torque performance or power factor, while the winding factor is constrained as above 0.866. Table II lists the optimal slot-pole combinations with decoupled windings. It should be mentioned that the slot-pole combinations with unity pole-pair of windings are excluded since such slot-pole combinations exhibit lengthy end-winding. Among the machines with the same number of stator slots Q_s and gear ratio G_{rI} in Table II, the one with highest gear ratio G_{rII} is selected for further analysis as it produces higher output torque as compared to the others. The selected machines 1 to 8 (i.e., M1–M8) are highlighted in light green in Table II. For a fair comparison, all the machines are designed to have the same outer stator diameter of 210 mm, stack length of 80 mm, PM volume and electric loading.

The main performances of eight machines are summarized in Table III. As can be seen, when the machines have the same Q_s, i.e., M1 and M2, M4 and M5, M6, M7 and M8, the one with higher gear ratio G_{rII} can produce higher average torque of inner rotor T_{av_inner} and outer rotor T_{av_outer}, despite having lower gear ratio G_{rI}. It is because G_{rII} of MGM part is involved in torque production of both inner and outer rotors but G_{rI} of PMV part is involved in only the outer rotor. As a result, M2, M3, M5, and M8 can produce higher torque, as highlighted in light orange in Table III.

Furthermore, due to higher G_{rII}, M3 and M8 exhibit higher output torques at the expense of little power factor, as compared with M2 and M5. Compared to M8, M3 can produce even better torque performance mainly because M8 suffers from more severe saturation and flux leakage due to its larger Q_s and P_{or} in a given size. On the other hand, among all the machines, M3 exhibits lower torque ripple and no unbalanced magnetic force (UMF), which are desirable for low-noise and low-vibration operation. Considering all the above factors, M3 (bolded in Table II and Table III) is selected for further investigation and experimental prototyping.

V. Performance Comparison and Evaluation

To evaluate the electromagnetic performances of the presented machine, a quantitative comparative study is conducted between the presented machine and the regular one in Fig. 2(a) [12, 18]. For a fair comparison, two machines are globally optimized to maximize total torque, power factor and efficiency under the same machine diameter, stack length, slot filling factor, and current density. The key specifications of the two machines are listed in Table IV.

TABLE IV
Main Specifications of Two Machines

Parameters	Regular machine	Presented machine
Stator outer diameter (mm)	210	
Stator inner diameter (mm)	70	
Outer airgap length (mm)	1.0	
Inner airgap length (mm)	1.0	
Stack length (mm)	80	
Current density (Arms/mm^2)	5	
Rated current of winding I (A)	12	
Rated current of winding II (A)	24	
Rated speed of inner rotor (r/min)	300	
Rated speed of outer rotor (r/min)	-200	
PM material	N40UH	
Steel material	35CS250	
Number of stator slots	48	24
Pole-pair of winding I	28	4
Pole-pair of winding II	11	2
Pole-pair of PMs in outer rotor	28	20
Number of steel segments in outer rotor	28	40
Number of iron poles in inner rotor	17	18
Number of turns per phase (winding I)	96	96
Number of turns per phase (winding II)	144	64
PM volume (L)	0.248	0.209

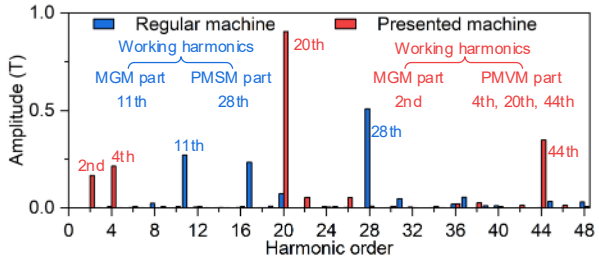

Fig. 5. Harmonic spectrum of flux density in outer airgap.

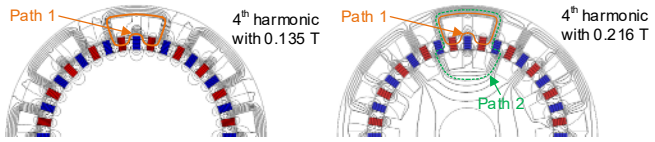

Fig. 6. Flux lines. (a) Without inner rotor. (b) With inner rotor.

A. Airgap Flux Density

Fig. 5 shows the harmonic spectrums of flux density in outer airgap of two machines. In terms of the MGM parts of two machines, the working harmonic of the regular machine is 11th with 0.271 T and that of the presented machine is 2nd with 0.167 T. The equivalent flux densities of MGM parts in two machines for torque generation are $G_{or\_WII} \times B_g$, i.e., (28/11) × 0.271 T = 0.69 T for the regular machine and (20/2) × 0.167 T = 1.67 T for the presented machine. On the other hand, the PMSM part of regular machine has only the 28th working harmonic with 0.509 T, while the PMVM part of the presented machine has working harmonics 4th with 0.216 T, 20th with 0.905 T and 44th with 0.348 T. The equivalent flux density of PMSM part for the regular machine is 0.509 T, while that of PMVM part for the presented machine is $G_{or\_WII} \times B_g(4^{th}) + B_g(20^{th}) - P_{or}/(P_{or} + Q_s) \times B_g(44^{th})$ = (20/4) × 0.216 + 0.905 - (20/44) × 0.348 = 1.83 T. As a result, the presented machine

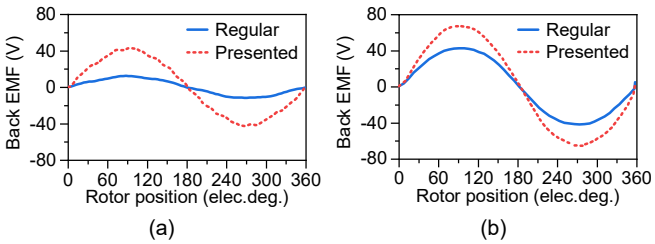

Fig. 7. No-load back-EMF waveforms. (a) Winding I. (b) Winding II.

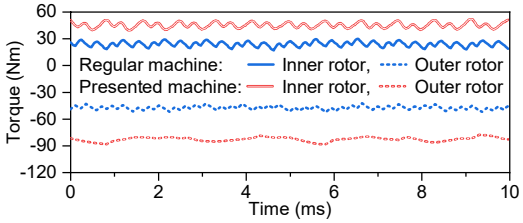

Fig. 8. Steady torque waveforms.

TABLE V
PERFORMANCE COMPARISON OF TWO MACHINES

Performance items	Regular machine	Presented machine
E_{WI} (V)	11.7	41.8
THD of E_{WI}	4.6	3.3
E_{WII} (V)	43.7	67.2
THD of E_{WII}	3.1	3.6
$T_{av\ outer}$ (Nm)	48.3	83.8
$T_{av\ inner}$ (Nm)	23.5	45.1
T_{rip_outer} (%)	19.5	13.9
T_{rip_inner} (%)	54.3	28.9
$P_{f\ WI}$	0.99	0.99
$P_{f\ WII}$	0.76	0.86
Copper loss (W)	197.2	278.4
Core loss (W)	36.9	61.9
PM loss (W)	10.0	3.9
Efficiency (%)	87.75	90.21
Output power (W)	1749.7	3171.7
Torque density (Nm/L)	25.9	46.5
Power density (kW/L)	0.63	1.15
PM volume (L)	0.248	0.209
Torque/PM volume (Nm/L)	289.5	616.7

can produce much higher equivalent flux densities both in the MGM part and PMVM part than of the regular machine. Thus, the presented machine can potentially generate larger back-electromotive force (EMF), torque and power than the regular counterpart.

On the other hand, the PMVM part of the presented machine benefits from the flux-bridge effect to produce higher amplitude of 4th working harmonic since the inner rotor functions can serve as the flux bridge to provide additional magnetic flux path. The flux lines of the presented machine with and without inner rotor is plotted in Fig. 6. Apart from magnetic path 1 (marked by orange line), the inner rotor provides the additional magnetic path 2 (marked by green line) for 4th working harmonic and hence the amplitude of 4th harmonic is boosted. As a result, the flux-bridge effect helps to improve the torque output of the PMVM part so as the overall torque of the presented machine.

B. No-Load Back-EMF

When the outer rotor and inner rotor rotate at the rated speeds of 200 r/min in clockwise and 300 r/min in counterclockwise, respectively, the no-load back-EMF waveforms of two

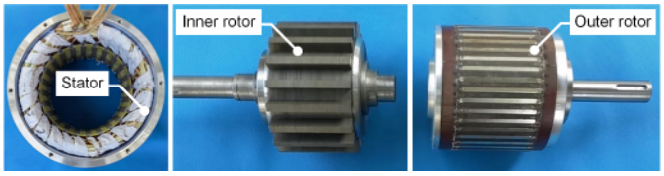

Fig. 9. Experimental prototype.

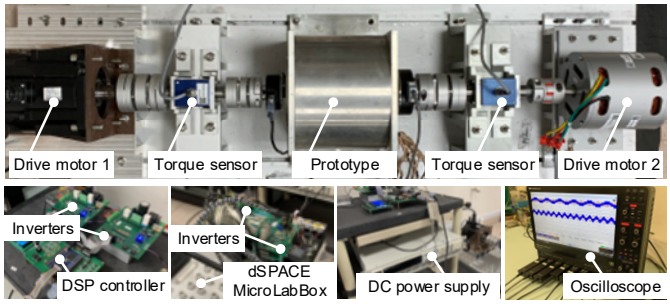

Fig. 10. Experimental test rig and key equipment.

machines are analyzed in Fig. 7. The fundamental amplitude and the total harmonic distortion (THD) of two windings are listed in Table V. Due to higher equivalent airgap flux density, the fundamental no-load back-EMF of the presented machine is significantly enhanced from 11.7 V to 41.8 V for winding I and 43.7 V to 67.2 V for winding II, as compared to the regular counterpart.

C. Torque Characteristic

Fig. 8 shows the torque waveforms of two machines at the rated conditions. The average torques of two rotors in the presented machine are significantly improved compared to those in the regular machine. Specifically, the torque of outer rotor is enhanced from 48.3 Nm to 83.8 Nm (i.e., 73.5% increase), while that of inner rotor is enhanced from 23.5 Nm to 45.1 Nm (i.e., 91.9% increase). Meanwhile, the torque ripples in the presented machine are suppressed from 19.5% to 13.9% in the outer rotor, and from 54.3% to 28.9% in the inner rotor, compared to the regular machine.

D. Other Performances and Discussion

Table V summarizes the power factor, losses, efficiency, and other key performances of presented machine and regular machine at rated condition. The power factors of winding I in both machines are very high (i.e., 0.99), which are higher than the power factors of winding II. It is mainly because the gear ratio G_{rI} of PMVM part is lower than gear ratio G_{rII} of MGM part. Besides, the power factor of winding II in the presented machine is higher than of the regular machine (i.e., 0.86 vs. 0.76). It is because the presented machine exhibits higher back-EMF of winding II than the regular ones. In terms of efficiency, the presented machine exhibits higher efficiency than the regular machine (i.e., 90.21% vs. 87.75%), owing to higher output torque and power. Compared to regular machine, the presented machine has about 82.5% higher power density (i.e., 1.15 kW/L vs. 0.63 kW/L) and 16.1% lower PM consumption (0.209 L vs. 0.248 L), showing that the presented machine also exhibits better PM utilization.

VI. EXPERIMENTAL VALIDATION

To validate the foregoing analysis and the proposed concepts, an experimental prototype of the presented CR-BIFM

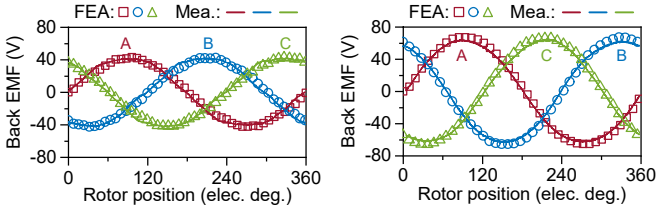

Fig. 11. Experimental results of no-load back EMF in comparison with FEA-predicted ones. (a) Winding I. (b) Winding II.

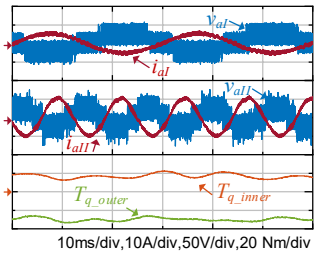

Fig. 12. Measured waveforms of current, voltage and torque.

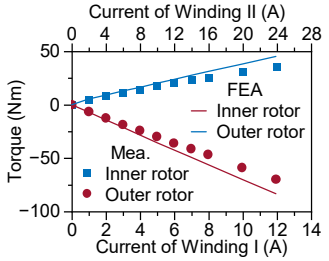

Fig. 13. Experimental results of torques versus current.

machine is manufactured and tested. Fig. 9 shows the prototype including the stator, inner rotor, and outer rotor. Fig. 10 presents the test rig for the experimental test and its key equipment. Two drive motors, which rotates reversely to provide driving torques for the prototype, are controlled by the TMS320F28335 controller and two three-phase voltage source inverters. The prototype, working in the generator mode, is controlled by dSPACE MicroLabBox and two three-phase voltage source inverters. All the inverters are connected in the same DC power supply, and thus the power generated from prototype can be utilized to supply the drive motors. The torques measured via two HBM torque sensors T21WN, currents and voltage measured via current and voltage probes are captured and displayed in the oscilloscope Lecroy-MDA 8058HD.

The experimental no-load back-EMF waveforms are obtained as shown in Fig. 11. When the outer rotor rotates in clockwise at rated 300 r/min and inner rotor rotates in counter-clockwise at rated 200 r/min, the no-load back EMFs of two windings are measured and compared with FEA-predicted ones. Good agreement can be observed between the FEA and experimental results, with about 5.5% discrepancy in the fundamental component. Under load conditions, the performances of the prototypes at different output currents are measured. Fig. 12 shows the measured waveforms of current (i_{aI}, i_{aII}), voltage (v_{aI}, v_{aII}) and torque (T_{q_inner}, T_{q_outer}) when the amplitude of i_{aI} and i_{aII} are 5 A and 10 A, respectively. The measured torques T_{av_outer} and T_{av_inner} are -30.12 Nm and 17.26 Nm, with the discrepancies of 15.3% and 13.7% in comparison with FEA results, respectively. The discrepancy may be mainly due to the mechanical loss and the end-winding effects. The torques of the prototype at different currents are presented in Fig. 13, where the amplitude of i_{aII} is twice larger that of i_{aI} to maintain the same current density of two windings. As can be seen, the measured and FEA-predicted torques are in acceptable agreement.

VII. Conclusion

In this paper, the CR-BIFM machine with open-slot structure is presented for wind turbines with improved wind energy harvesting capability. The results show the presented machine provides higher torque/power density, higher efficiency, higher power factor, and higher PM utilization than the regular counterpart mainly due to the dual flux-modulation effect and flux-bridge effect of the presented machine. The decoupling analysis of the presented machine is studied in depth with the consideration of the influence of both stator and rotors from the perspective of air-gap modulated magnetic field, while the conditions for achieving decoupled windings with low coupling degree are concluded. The presented decoupling analysis in this paper is generic and can be extended to analyze other types of BIFM machines as well as machines with multiple sets of windings. Finally, an experimental prototype of the presented machine is manufactured and tested to validate the analysis.

References

[1] V. Yaramasu, B. Wu, P. C. Sen, S. Kouro, and M. Narimani, "High-power wind energy conversion systems: State-of-the-art and emerging technologies," *Proc. IEEE,* vol. 103, no. 5, pp. 740-788, May 2015.

[2] H. Chen, Y. Zuo, K. T. Chau, W. Zhao, and C. H. T. Lee, "Modern electric machines and drives for wind power generation: A review of opportunities and challenges," *IET Renew. Power Gener.,* vol. 15, no. 9, pp. 1864-1887, Oct. 2021.

[3] Y. Zou, M. E. Elbuluk, and Y. Sozer, "Simulation comparisons and implementation of induction generator wind power systems," *IEEE Trans. Ind. Appl.,* vol. 49, no. 3, pp. 1119-1128, Mar. 2013.

[4] S. Toma, L. Capocchi, and G. A. Capolino, "Wound-rotor induction generator inter-turn short-circuits diagnosis using a new digital neural network," *IEEE Trans. Ind. Electron.,* vol. 60, no. 9, pp. 4043-4052, Sept. 2013.

[5] N. K. Swami Naidu, and B. Singh, "Doubly fed induction generator for wind energy conversion systems with integrated active filter capabilities," *IEEE Trans. Ind. Inform.,* vol. 11, no. 4, pp. 923-933, Aug. 2015.

[6] D. Zhou, F. Blaabjerg, T. Franke, M. Tonnes, and M. Lau, "Comparison of wind power converter reliability with low-speed and medium-speed permanent-magnet synchronous generators," *IEEE Trans. Ind. Electron.,* vol. 62, no. 10, pp. 6575-6584, Oct. 2015.

[7] A. W. Manyonge, R. Ochieng, F. Onyango, and J. Shichikha, "Mathematical modelling of wind turbine in a wind energy conversion system: Power coefficient analysis," *Appl. Math Sci.,* vol. 6, no. 91, pp. 4527-4536, Jan. 2012.

[8] R. W. Y. Habash, V. Groza, Y. Yang, C. Blouin, and P. Guillemette, "Performance of a contrarotating small wind energy converter," *Int. Sch. Res. Network,* vol. 2011, pp. 1-10, Mar. 2011.

[9] P. S. Kumar, A. Abraham, R. J. Bensingh, and S. Ilangovan, "Computational and experimental analysis of a counter-rotating wind turbine system," *J. Sci. Ind. Res.,* vol. 72, pp. 300-306, May 2013.

[10] C. Shin, *Multi-unit rotor blade system integrated wind turbine*, U. S. Patent 5876181, 1999.

[11] S. N. Jung, T.-S. No, and K.-W. Ryu, "Aerodynamic performance prediction of a 30 kW counter-rotating wind turbine system," *Renew. Energy,* vol. 30, no. 5, pp. 631-644, Apr. 2005.

[12] X. Luo, and S. Niu, "A novel contra-rotating power split transmission system for wind power generation and its dual MPPT control strategy," *IEEE Trans. Power. Electron.,* vol. 32, no. 9, pp. 6924-6935, Sept. 2017.

[13] S. Sasaki, "Toyota's newly developed hybrid powertrain," in *IEEE Int. Symp. Power Electron.*, Jun. 1997, pp. 17-22.

[14] X. Ren, D. Li, R. Qu, W. Kong, X. Han, and T. Pei, "Analysis of spoke-type brushless dual-electrical-port dual-mechanical-port machine with decoupled windings," *IEEE Trans. Ind. Electron.,* vol. 66, no. 8, pp. 6128-6140, Aug. 2019.

[15] X. Ren, D. Li, R. Qu, and T. Zou, "A brushless dual-mechanical-port dual-electrical-port machine with spoke array magnets in flux modulator," *IEEE Trans. Magn.,* vol. 53, no. 11, pp. 1-6, Nov. 2017.

[16] Z. Liang, X. Ren, D. Li, R. Qu, and X. Han, "Analysis of a Spoke-Array Brushless Dual-Electrical-Port Dual-Mechanical-Port Machine With Reluctance Rotor," *IEEE Trans. Ind. Electron.,* vol. 68, no. 4, pp. 2999-3011, Apr. 2021.

[17] Y. Liu, S. Niu, and W. Fu, "Design of an electrical continuously variable transmission based wind energy conversion system," *IEEE Trans. Ind. Electron.,* vol. 63, no. 11, pp. 6745-6755, Nov. 2016.
[18] Y. Wang, S. Niu, and W. Fu, "Electrical-continuously variable transmission system based on doubly fed flux-bidirectional modulation," *IEEE Trans. Ind. Electron.,* vol. 64, no. 4, pp. 2722-2731, Apr. 2017.
[19] H. Chen, A. M. E.-. Refaie, Y. Zuo, S. Cai, S. Xie, and C. H. T. Lee, "Evaluation of a contra-rotating flux-modulated machine featured With dual flux-modulation for wind power generation," *IEEE Trans. Ind. Electron.,* vol. 69, no. 9, pp. 8770-8781, Sept. 2022.
[20] N. Bianchi, S. Bolognani, and M. D. Pre, "Magnetic loading of fractional-slot three-phase PM motors with nonoverlapped coils," *IEEE Trans. Ind. Appl.,* vol. 44, no. 5, pp. 1513-1521, Sept. 2008.

Libing Cao (M'20) received the B.Eng. degree in electrical and electronic engineering from Zhejiang University, Hangzhou, China, in 2016, and the Ph.D. degree in electrical and electronic engineering from The University of Hong Kong, Pokfulam, Hong Kong, in 2020. He is currently a Postdoctoral Research Fellow with Nanyang Technological University, Singapore.

Guanghui Yang received the B.Sc degree in electrical enginerring from Southeast Univeristy, China, in 2019. He is currently working toward the Ph.D. degree in electrical engineering with the College of Electrical Engineering with Zhejiang Univeysity, Hangzhou, China.

Yuefei Zuo (M'18) received the B.Sc. and the Ph. D. degrees in electrical engineering and automation from Nanjing University of Aeronautics and Astronautics, Nanjing, China, in 2010 and 2016, respectively. He is currently a Postdoctoral Research Fellow with Nanyang Technological University, Singapore.

Yaojie He received the B.Sc. degree in electrical engineering and automation from the College of Electrical and Information Engineering, Hunan University, Changsha, China, in 2018. He is currently working toward the Ph.D. degree with the School of Electrical and Electronics Engineering, Nanyang Technology University, Singapore

Chenhao Zhao received his B.Eng. degree in Electrical and Electronic Engineering from the University of Nottingham, Ningbo, China in 2020, and the M.Sc. degree in power engineering from Nanyang Technological University, Singapore in 2021. He is currently working toward the Ph.D. degree in the School of Electrical and Electronic Engineering, Nanyang Technological University,Singapore.

Shuangchun Xie received his B.Sc. degree in electrical engineering and automation from Nanjing University of Aeronautics and Astronautics, Nanjing, China, in 2017. He is currently working toward the Ph.D. degree in School of Electrical and Electronic Engineering, Nanyang Technological University, Singapore

Christopher H. T. Lee (SM'18) received his B.Eng. degree and Ph.D. degree both in electrical engineering from Department of Electrical and Electronic Engineering, The University of Hong Kong, Hong Kong, in 2009 and 2016, respectively. He currently serves as an Assistant Professor at Nanyang Technological University, Singapore and Honorary Assistant Professor at The University of Hong Kong, Hong Kong. He was a Postdoctoral Fellow and then a Visiting Assistant Professor at Massachusetts Institute of Technology, United States. He is an Associate Editor for IEEE Transactions on Industrial Electronics, IEEE Transactions on Energy Conversion, IEEE Access and IET Renewable Power Generation.